Journal of Inorganic and Organometallic Polymers and Materials (2022) 32:2040–2055
https://doi.org/10.1007/s10904-022-02261-9

Biodegradable Polyvinyl Alcohol/Carboxymethyl Cellulose Composite Incorporated with L-Alanine Functionalized MgO Nanoplates: Physico-chemical and Food Packaging Features

Yamanappagouda Amaregouda[1] · Kantharaju Kamanna[1] · Tilak Gasti[2]

Received: 19 December 2021 / Accepted: 16 February 2022 / Published online: 2 March 2022

Abstract
In the present work, MgO NPs have been prepared by novel biogenic method using agro-waste WELFSA and their surface was modified using L-alanine under microwave irradiation. Then the effect of L-alanine functionalized MgO NPs (1, 3 and 5 wt%) on the polyvinyl alcohol/carboxymethyl cellulose (PVA/CMC) matrices blended to investigate physico-mechanical properties of the as-prepared nanocomposite films using various techniques. The SEM image showed homogenous distribution of plate-like nanostructure of MgO-L-alanine in the doped polymeric film matrices. The molecular interactions between the nanocomposite film components were confirmed by the FT-IR spectra. The tensile strength of PVA/CMC nanocomposites (NCs) was improved from 15.52 ± 0.27 to 50.32 ± 0.61 MPa, when filled with 5 wt% of MgO-L-alanine. Moreover, the UV rays blocking, hydrophobicity, water vapor transmission, moisture retention capacity and thermal stability of the PVA/CMC blend was greatly enhanced by the incorporation of MgO-L-alanine NPs. Furthermore, overall migration limit of PVA/CMC NCs films against their food simulants were found below the permitted limit of 10 mg/dm^2. In addition, PVA/CMC NCs films had shown high antimicrobial against *Escherichia coli* and *Candida albicans* microbes and also showed excellent antioxidant activity against DPPH free radicals assay. Further, the prepared films undergo more than 30% soil degradation rate, when buried in untreated soil. Overall, these results suggest that the prepared PVA/CMC NCs films could be employed as a promising candidate for food packaging applications.

Keywords Polyvinyl alcohol · Carboxymethyl cellulose · Magnesium oxide nanoparticles · L-Alanine · Biodegradable · Food packaging

1 Introduction

Since from last few decades single used plastics (SUP) and fossil-based plastics imposed more negative impact on environmental pollution. Environmental pollution, fossil resources depletion, and associated global warming are the key drivers that are advocating a shift from SUP and fossil-based polymers in to biodegradable polymers [1–3]. Because of their non-biodegradability and non-renewability, petrochemical-based packaging materials pose a threat to the environment [4]. As a result, biodegradable films are employed in food packaging [5, 6]. Food packaging is essential for protecting food from the elements such as moisture, as well as providing nutrition, taste and ingredients to consumers [7]. Polyvinyl alcohol (PVA) is a water-soluble synthetic polymer [8, 9], utilized in food and pharmaceutical packaging, cling film, and other applications because of its non-toxic, biodegradable, non-polluting, and excellent film-forming properties [10, 11]. In spite of these interesting properties, PVA film has some limitations that include low tensile strength and high water solubility. In order to overcome some of these limitations, PVA films often blended with other natural polymers such as starch [12], chitosan [13, 14], pectin [15], gelatin [16], and cellulose derivatives [17]. Among the several natural polymers doped with PVA, carboxymethyl cellulose was extensively blended to improve

✉ Kantharaju Kamanna
kk@rcub.ac.in

[1] School of Basic Sciences: Department of Chemistry, Rani Channamma University, Vidyasangama, P-B, NH-4, Belagavi, Karnataka 591156, India

[2] Department of Chemistry, Karnatak University, Dharwad 580003, India

mechanical, optical, thermal, and water barrier properties of PVA are well documented [18, 19].

Carboxymethyl cellulose (CMC) is derivative of cellulose, which is soluble in water. The CMC is largely used as thickening agent in wide range of pharmaceutical, food, home, and personal care applications as well as in the paper industries, water treatment, and mineral processing industries [20]. CMC is largely employed in the food packaging applications due to its degradability, non-toxicity, and biocompatibility. However, it is important for any packaging materials that do not only protect the packed food product from atmospheric conditions, but also extend its shelf life. The most familiar way to protect and extend the shelf life of packed food product is incorporation of bio-active additives or fillers into the film matrices. There are several ingredients readily used as bio-active components such as plant polyphenols and inorganic metal nanoparticles. For instance, metal oxide nanofillers, such as CuO [21, 22], MnO_2 [23], ZnO [24–26], Fe_2O_3 [27], MgO [28], and other metal oxide NPs, are added in to polymer matrix to increase mechanical and barrier characteristics as well as other functions like antibacterial activity and medicinal properties [29, 30].

Nanoparticles are most attracted additives in the food packaging applications, due to their high resistance to the food borne pathogens and ability to inhibit the oxidation process of the food products. Nowadays several nanoparticles are synthesized through various experimental techniques such as chemical reduction method and green methods. However, the use of chemical reducing agents such as sodium borohydride, hydrazine hydrate, trisodium citrates, hydroxylamine hydrochloride methods cause deposition of harmful toxic components on the surface of the nanoparticles causes serious health effect, when we used in food systems [31]. As a result, the green method synthesized nanoparticles was established an ecologically benign synthetic approach. Such methods for synthesizing nanoparticles found are safe, cost effective, and efficient, as well as environmentally friendly. In this regard, several researchers focusing on the utilization of green method reducing sources such as grape juice, sonochemical, light irradiation and date palm extract for the synthesis of nanoparticles [32–41].

Among various kind of metal nanoparticles, MgO NPs also have unique physico-chemical properties such as physical strength, stability, flame resistance, dielectric resistance, mechanical strength, and high optical transparency [42]. Biogenic synthesis of MgO NPs has received a lot of interest as a consistent, sustainable, and environmentally acceptable method [43]. Meanwhile, MgO NPs play an effective role in reinforcing polymers due to interaction between nano-sized species that form a percolated network via hydrogen bonding. However, MgO NPs have a strong tendency to agglomerate, as a result, attaining homogenous dispersion of them on the polymer matrix is quite difficult. Hence, surface modification of MgO NPs with a biologically active organic compound is a promising route for increasing their dispersion and stability in the polymer matrices. L-Alanine is a bio-organic molecule, it contains both amino and carboxyl groups. The biodegradability, biocompatibility, nontoxic, antibacterial, antioxidant, and eco-friendly properties of MgO NPs modified with L-alanine have been demonstrated [44–49]. In the current study, L-alanine was chosen for chemical and physical surface modification of the MgO nanostructure, and blended with polymers to achieve better properties.

To the best of our knowledge, literature about PVA/CMC blended film reinforced with MgO-L-alanine is not available. Therefore, the purpose of the present work is to characterize micro-structural, physical, mechanical, optical, thermal, antimicrobial, antioxidant and barrier properties of the PVA/CMC blend films reinforced with different amounts of MgO-L-alanine films prepared by a solution casting method, and these films can be emerged as a food packaging applications.

2 Material and Methods

2.1 Materials and Reagents

Lemons were collected from the local market in Belagavi, Karnataka, India. Magnesium nitrate hexahydrate ($Mg(NO_3)_2{\cdot}6\ H_2O$) and 2,2–diphenyl–1–picrylhydrazyl (DPPH) were supplied by Sigma-Aldrich, India. L-Alanine was procured from Avra, India, Polyvinyl alcohol (MW: 125,000 g mol^{-1}) and carboxymethyl cellulose (MW: 250,000 g mol^{-1}) obtained from HIMEDIA, India. Ethanol and acetic acid were purchased from SD-fine Chemicals, India. Double distilled water was utilized throughout the experiment. All the chemicals and compounds were used analytical grade, and used directly as received without further purification.

2.1.1 Preparation of Water Extract of Lemon Fruit Shell Ash (WELFSA)

WELFSA is prepared by our previous reported procedure [50], briefly, lemon fruit (Citrus limon) shells are collected from local juice center, rinsed with distilled water, dried in the sun light, and then burned to ash with a Bunsen burner. Thereafter, the burnt ash (5 g) was soaked for around 2 h in distilled water (100 mL) before being filtered. The filtrate is known as the WELFSA solution and observed pH of 11.24.

2.1.2 Green Method Synthesis of MgO NPs

The 100 mL of above prepared 5% WELFSA solution was boiled at 70 ± 2 °C with constant stirring, to this 0.1 M of

magnesium nitrate hexahydrate was added, and vigorously stirred until a white precipitate formation. The reaction allowed to settle precipitation, then filtered and rinsed with distilled water: ethanol (1:1) mixture, until the filtrate solution showed neutral pH. The resulted white precipitate was dried at 80 °C for 6 h in a hot air oven before being calcined at 600 °C for 4 h [43].

2.1.3 Modification of MgO Nanoplates

Initially, 0.05 g MgO nanoplates suspended in a 5 mL ethanol and were sonicated for 20 min before being treated with 0.2 g L-alanine amino acid (4 mmol) in double distilled water/ethanol solvents (4:1). The mixture was then transferred into RB flask and heated in a microwave oven with an output power of 800 W for 10 min at 120 °C [51]. After that, the reaction mixture was allowed to reach room temperature, the modified MgO nanoplates were centrifuged and washed with double distilled water and ethanol mixture, and finally vacuum-dried at 80 °C.

2.1.4 Fabrication of PVA, PVA/CMC, PVA/CMC/MgO-L-Alanine NCs Films

The films were prepared through solvent casting technique. Briefly, 2 g of PVA and 0.5 g of CMC were each dissolved separately in 100 mL and 50 mL of water respectively. Then both the solutions were mixed and blended for a 15 min, thereafter, the different weight percentage of (1, 3 and 5 wt%) MgO-L-alanine NPs dispersed in water through ultrasonication was added to it, and stirred for 24 h to achieve homogeneity of the polymer NCs, finally the mixture was sonicated further more. The resultant solution was poured onto a petridish and dried at 50 °C for 5 h. The dried films were peeled off, and placed in a zip lock pouch to be studied late. The pure PVA film was made using the above-mentioned process without use of the CMC or MgO nanoplates. The photographs of the prepared films are shown in the Fig. 1.

Fig. 1 Photographs of PVA, PVA/CMC, PCM-1, PCM-2 and PCM-3 films

2.2 UV–Vis Light Absorbance, Transmittance, Transparency and Opacity Value

UV–Vis spectroscopy was used to investigate the formation of MgO nanoplates, surface modification of the MgO nanoplates, and light barrier properties determination (opacity, transparency, and percent transmittance) of the prepared nanocomposite films (Shimadzu, UV-1800, USA). The film sample (4 cm) was placed in a sample cell, and the spectrum was recorded using air as a standard reference between the wavelength ranges of 200–800 nm. For the same sample, three measurements were taken, and the findings data were expressed as mean standard deviation (n = 3). Equations (1) and (2) were used to measure the opacity and transparency of the prepared nanocomposite films respectively [52].

$$Opacity = \frac{Abs_{500}}{b} \tag{1}$$

where Abs_{500} the absorbance at 500 nm and b is the thickness of the film (nm).

$$Transparency\left(T_{600}\right) = \frac{-\log(\%T_{600})}{b} \tag{2}$$

where %T is the percentage transmittance at 600 nm and b is the film thickness in nm.

2.3 Attenuated Total Reflection (ATR)/Fourier-Transform Infrared (FT-IR) Spectroscopy

The prepared NCs films' FT-IR spectra were recorded using an attenuated total reflectance—Fourier transform infrared (ATR FT-IR) spectrometer (Thermo Scientific, Nicolet iZ10) between the wave number ranges from 4000 to 400 cm^{-1}.

2.4 X-ray Diffraction (XRD) Analysis

The crystalline and amorphous behavior of the synthesized MgO NPs, L-Ala functionalized MgO NPs, and prepared film samples were analyzed by X-ray diffraction (XRD) using a Rigaku Miniflex Diffractometer in reflection mode with Cu Kα radiation at an accelerating voltage of 30 kV with operating current of 10 mA and a scan speed of 2° min^{-1} from an angle (2θ) 10º to 80° [53].

2.5 Scanning Electron Microscopy (SEM) and Energy Dispersive X-ray (EDX)

The surface morphology of the NCs films were examined using a scanning electron microscopy (SEM) equipped with an energy dispersive X-rays (EDX) spectrometer from TESCAN (CZECH REPUBLIC), VEGA3. A thin palladium/platinum conductive coating was applied to the samples before they were further processed. The layer was developed using a sputter coating. The surface of the sample was viewed using a secondary electron detector with a 30 kV accelerating voltage [51, 54].

2.6 Thermal Analysis

The thermal stability and decomposition temperature of the prepared film samples were assessed by thermogravimetric analysis (TGA) (TA-SDT650 instruments, USA). The film sample (4–4.5 mg) was heated at a rate of 10 °C/min in the temperature range 25–600 °C under a nitrogen atmosphere (50 mL/min). The differential scanning calorimetry (DSC) was performed in an inert nitrogen atmosphere (50 mL/min), the 1.5–2.0 mg of film sample was enclosed in an aluminium crucible and heated at a rate of 10 °C/min from 25 to 400 °C [10].

2.7 Mechanical Properties

The prepared PVA/CMC/MgO-L-alanine NCs tensile characteristics are assessed using a computer-based DAK testing machine (UTM) in accordance with ASTM D882–91. The films were cut into rectangular pieces of 0.5 × 0.71 cm and evaluated at a crosshead speed of 1 mm/min with a gauge length of 5 cm [51]. The thickness of each film sample was taken into account throughout the testing, and an average reading was taken. The prepared films are showed 0.0090 ± 002 cm thickness on and average.

2.8 Soil Burial Degradation (SBD)

The prepared nanocomposite films' SBD was determined using a slight modified version of reported procedure [13]. The film sample (1.415 × 1.415 cm) was weighed after being dried at 80 °C. The weighed dry NCs film samples are buried at a depth of 10 cm in black soil, with 10 mL of water supplied every day for 10 days. After 10 days of treatment, the buried films were carefully removed, washed with water, and dried at 80 °C. The degraded samples' dry weights were measured, and the percentage degradation was calculated using Eq. (3).

$$SBD\,(\%) = \text{Soil burial degradation}\,(\%) = \frac{Initial_{wt} - Final_{wt}}{Initial_{wt}} \times 100 \quad (3)$$

2.9 Moisture Retention Capability (MRC)

The moisture retention capacity (MRC) of the prepared films was conducted using ASTM D570-98, before and after 24 h of drying in a 105 ± 2 °C oven. The weight of the film samples was calculated using Eq. (4) for the MRC (%) [55].

$$\text{MRC}\,(\%) = \text{Moisture retention capacity}\,(\%) = [W_f/W_i] \times 100 \quad (4)$$

where W_i and W_f are the weight of the films before and after drying respectively.

2.10 Water Vapor Transmission Rate (WVTR)

The developed films were assessed for their water vapor transmission rate (WVTR) using a modified version of a method described in the literature [25]. To conduct the test, 10 mL of DDI water was poured in a glass bottle with a 29.5 mm inner diameter, and the mouth of the glass bottle was wrapped with prepared films and tightened with Teflon tape. Before heating, the weight (Wi) of the bottle was recorded, and it was placed in a preheated hot air oven at 40 °C for 24 h. After 24 h in the oven, the sample bottle was weighed (Wf) again, and WVTR was estimated using Eq. (5) [56].

$$WVTR = Water\ vapor\ transmission\ rate = [W_i - W_f/A] \times T \quad (5)$$

where A is the area of the mouth of the bottle and T = 24 h.

2.11 Surface Wettability Test (SWT)

A water contact angle meter was used to assess the surface wettability of the developed films using the sessile drop technique (Kyowa Interface Science Co. Ltd., Tokyo). A micro syringe was used to drop 2 L of distilled water onto the film surface, which was put on the specimen holder. Preloaded software and a high–resolution camera were used to capture the contact angle between the film surface and the water droplet picture to determine the static water contact angle. For the same film sample, the water contact angle was measured for three times, and the mean and standard deviation were calculated [31].

2.12 Overall Migration Rate

The food compatibility of the developed nanocomposite films was determined gravimetrically by calculating the total migration rate of the film contents into food simulants as per

IS: 9485 (1998) recommendations. In each beaker, the film sample was immersed in 30 mL DDI water, 3% acetic acid, and 50% ethanol solutions and kept for 10 days in a hot air oven at 40 °C. The samples were dried and weighed again after 10 days. In milligrams per cubic meter, the film's total migration limit into the food simulants was measured [31].

2.13 Antioxidant Activity

The antioxidant activity of the prepared NCs films was determined using a DPPH (2,2-diphenyl-1-picrylhydrazyl) technique based on their free radical scavenging activity according to the procedure, 2 mL (1 mMol) of DPPH in methanolic solution and 1 mL of each sample solution (20, 40, 60, 80, and 100 g/mL) were mixed and incubated at room temperature for 30 min. The absorbance values at 517 nm of these incubated sample mixtures were measured using a UV–Vis spectrophotometer. The standard reference taken was ascorbic acid (AA), and the control was a blank DPPH solution. Three tests were performed on the same material, with the findings provided as mean SD using Eq. 6 to calculate scavenging activity of the DPPH [6].

$$DPPH\ radical\ scavenging\ activity\ (\%) = \frac{Abs_{control} - Abs_{sample}}{Abs_{control}} \times 100 \quad (6)$$

2.14 Antibacterial and Antifungal Activity

The prepared NCs films were tested for food pathogens, including Gram-negative bacteria (*E. coli*) antibacterial and antifungal activities (*C. albicans*) [57]. To begin, the pure colonies of the test organisms were inoculated into nutrient broth culture, which was then incubated for 24 h. In a nutshell, a stock solution was made by dissolving 10 mg of the NCs film sample in 10 µL of DMSO. In a test tube, 1.5 µL of brain heart infusions (BHI) agar and 10 µL of each *E. coli* and *S. aureus* suspension were mixed well, then 100 µL of NCs film samples from the stock solution were added and gently mixed. Colonies were counted as colony-forming units per mL (CFU/mL) after 24 h of inoculation at 37 °C. The above-mentioned procedure was used for antifungal (*Candida albicans* and *Candida tropicalis*) activity investigations also, but instead of BHI, sabotaged dextrose agar (SDA) was used, and the control was made as above but without the NCs film sample.

2.15 Statistical Analysis

One-way analysis of variance statistical analysis was used in the Origin–9 programme (Origin Lab USA). The data collection tests were done in triplicate and the average standard deviation (n = 3) was reported.

3 Result and Discussion

3.1 UV–Vis Light Absorbance, Transmittance, Transparency and Opacity Value

The UV–Vis absorption spectra indicated a characteristic maximum absorbance at 373 nm (WELFSA), 306 nm (MgO-L-alanine), and 260 nm (MgO NPs), correlating MgO and MgO-L-alanine semiconductor excitation via Surface Plasmon Resonance (SPR) observed (Fig. 2a) [58]. One of the most important characteristic designs of the films for specific food packaging categories is their UV–Vis light barrier, because it prevents or suppresses the oxidation of lipids, pigments, proteins, and vitamins. This trait is directly related to food shelf life, as it prevents unpleasant smells, colors, aromas, and nutrient loss, preserving the packed food's organoleptic and nutritional aspects. The absorption spectra of the prepared NCs films were shown in Fig. 2b [52]. There was no peak observed over 200–800 nm for PVA and PVA/CMC films due to the absence of MgO-L-alanine. However, for all NCs a characteristic peak was appeared at λ_{max} 357 nm due to the SPR of MgO-L-alanine. The spectral data indicated presence of MgO-L-alanine in the PVA/CMC matrix. The light transmittance of the NCs film was considerably reduced as the MgO-L-alanine content in the PVA/CMC matrix was increased. This reduction in the transmittance of both UV and visible light is associated with the interaction of MgO-L-alanine with the PVA-CMC matrix and is responsible for the compact and higher polymeric chain network preventing the passage of light and UV–Vis light (Fig. 2c) [21]. The transparency is a critical characteristic properties of a film, particularly when they are employed as packaging materials, and it has a direct impact on economic success and consumer acceptance [5]. A comparison between the transparency of pristine PVA, PVA/CMC, and PVA/CMC loaded with various concentration of MgO-L-alanine were demonstrated in Fig. 2d. The most transparent film is neat PVA and PVA/CMC films, when MgO-L-alanine is added to the PVA/CMC matrix, the transparency values decrease. This indicates that, the MgO-L-alanine fills the space between the polymer matrix chains, increasing the number of barriers that light may traverse. The prepared NCs film's opacity was determined by measuring transmittance at 600 nm. As can be seen, when MgO-L-alanine is added

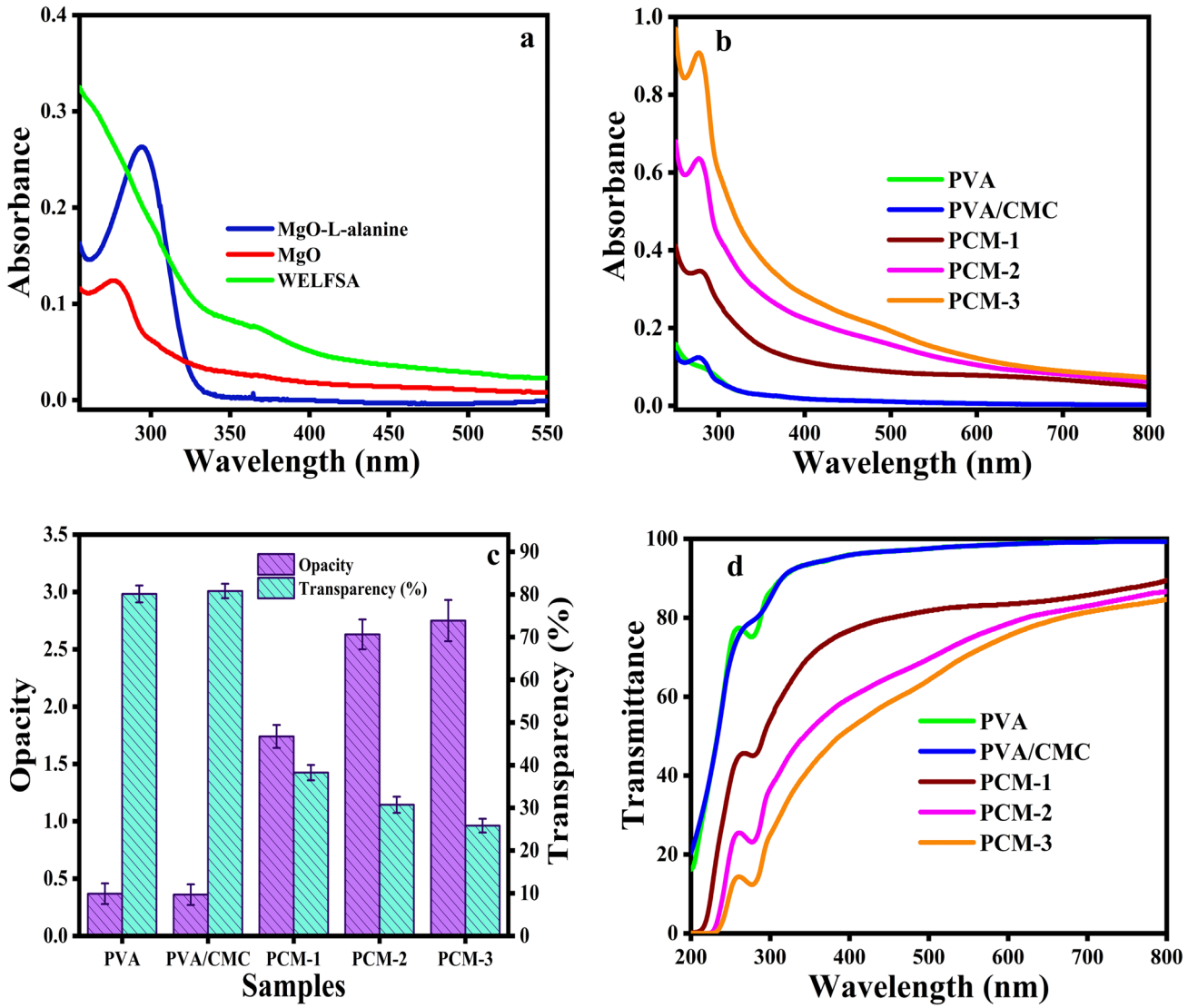

Fig. 2 **a** UV–Vis spectra of: green) WELFSA, red) MgO nanoplates and blue) MgO-L-alanine; Optical properties of the prepared films; **b** UV–Vis absorption, **c** Opacity at 500 nm and Transparency at 600 nm (mean ± SD, n = 3); **d** % Transmittance (Color figure online)

to the PVA/CMC matrix, the opacity value increases, and higher opacity value was observed at PCM-3 NCs film ($p < 0.05$), due to the densely packed plates of MgO-L-alanine particles, are mainly responsible for light path obstruction (Fig. 2d) [31].

3.2 Attenuated Total Reflection (ATR)/ Fourier-Transform Infrared (FT-IR) Spectroscopy

FT-IR spectra of MgO and MgO-L-alanine NPs are illustrated in Fig. 3 [58, 59]. In the case of MgO NPs, the peak at 3239.3 cm^{-1} and at 1628.7 cm^{-1} is of O–H stretching vibration and C=O stretching vibrations respectively. A strong peak at 580 cm^{-1} indicates the presence of MgO, and also the broadband spectrum at 3282 cm^{-1}can be referred to as the OH band group of MgO-L-alanine. Moreover, at 1631.7 cm^{-1} peak corresponds to MgO-L-alanine is due to the symmetric C=O stretching from the COOH group. This broad peak displays slight shifts to a lower wavelength at approximately 1614 cm^{-1} for the carboxylic group (R-OOH) of the MgO-L-alanine. Furthermore, peak at 1614 cm^{-1} determines the binding of L-alanine on the surface of MgO NPs through chemisorption of the carboxylic group. The peak at 1378 cm^{-1}can be ascribed to the asymmetric stretching of C–O from the carboxylic group. The intense peak observed at approximately 580 cm^{-1} in MgO-L-alanine could be assigned to the Mg–O stretching vibrational mode. Hence, L-alanine binds to the MgO surface through carboxylic group. Figure 3 represents prepared films ATR-FT-IR spectra of

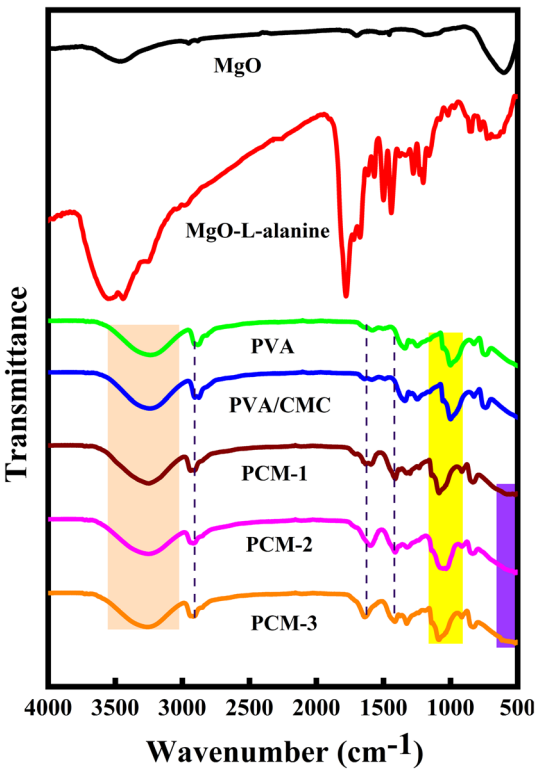

Fig. 3 FT-IR spectra of MgO, MgO-L-alanine, pure PVA, PVA/CMC and NC film

PVA, PVA/CMC and PVA/CMC NCs films showed peaks at 3286.4, 3291.1 and 3259.6 cm^{-1} indicating NH_2 groups and free hydroxyl groups owing to the strong intermolecular and intramolecular bonds [17, 18]. The addition of MgO-L-alanine in the PVA/CMC matrix causes a slight variation of the intensity of O–H stretching. It can be ascribed to the interface between the hydroxyl group on the surface of MgO-L-alanine and the hydroxyl group in the PVA/CMC matrix. Furthermore, PVA/CMC/MgO-L-alanine NCs films exhibits NH_2 group stretching vibrations at 3273.0 cm^{-1}. The shifting of PVA/CMC hydroxyl peak at 2900 cm^{-1} is not obvious with addition of different concentration of MgO-L-alanine to the PVA/CMC matrix. Because MgO-L-alanine and PVA/CMC have strong overlap in the region of O–H stretching. The peaks at 2905.9 and 2915.2 cm^{-1} can be assigned to C–H stretching vibrations, peak at 1634.9 cm^{-1} corresponds to C=O stretching of carboxyl group. The wavenumber corresponds to 1232.2 and 1245.6 cm^{-1} stretching vibration of C–O and C–OH out of plane bending mode. The regular PVA/CMC bonds were noticed in the PCM-1, PCM-2 and PCM-3 films spectra, which indicated that the addition of MgO-L-alanine had no major influence on the molecular structure of the PVA/CMC films.

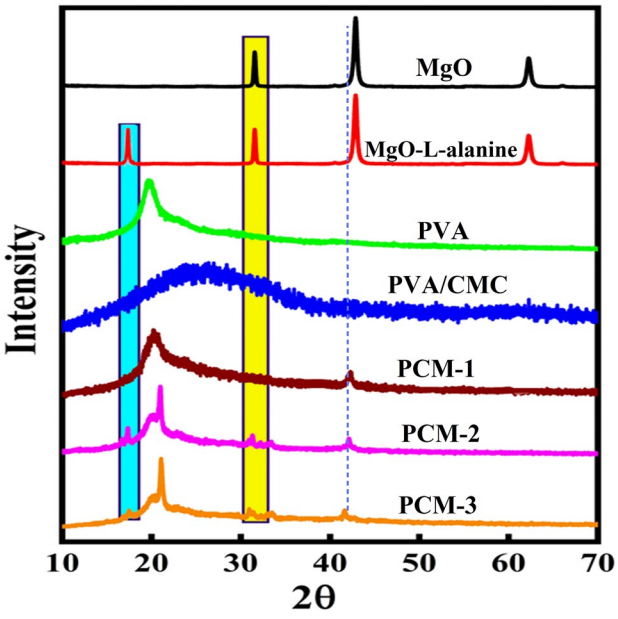

Fig. 4 XRD spectra of MgO, MgO-L-alanine, pure PVA, PVA/CMC and NC films

3.3 X-ray Diffraction (XRD) Analysis

Figure 4 shows the XRD pattern of MgO NPs. The diffraction peaks are indexed into the face-centered cubic MgO structure and are in good agreement with the Joint Committee for Powder Diffraction Studies (JCPDS) File No. 89-7746 [58]. The observed peaks at $2\theta = 36.63$, 42.45, 61.84, 74.11, and 78.04 are connected with the [111], [200], [220], [311], and [222] planes, respectively, which are in good agreement with the literature. Further, there were no distinctive peaks of other contaminants in the diffraction pattern, indicating MgO NPs, prepared using novel route produce high purity. The crystallite size of the prepared MgO NPs is ranged from 38.3 to 83.2 nm with an average was measured by using Debye–Scherrer equation ($D = 0.9\lambda/\beta \cos\theta$). Similarly, the XRD pattern of MgO-L-alanine shows the crystalline structure like MgO NPs with an additional peak of L-alanine at $2\theta = 18°$ [59]. Furthermore, the XRD patterns of PVA, PVA/CMC, and PVA/CMC NCs films are shown in Fig. 4. The maximum intensity diffraction peak exists around $2\theta = 20°$ in CMC/PVA blend, which indicates its semi-crystalline structure and it is comprised of both crystalline and amorphous regions. In addition, the broad peak was observed in the XRD pattern for CMC/PVA in other reported works [18, 19]. This peak is somewhat higher than the main peak of pure PVA, which is 19.5° [19] due to the addition of CMC. These XRD data suggests a great interaction between PVA and CMC taking place in film. Adding of different % content of MgO-L-alanine showed L-alanine peak at $2\theta = 18°$ and shift 2θ value of CMC/PVA to slightly

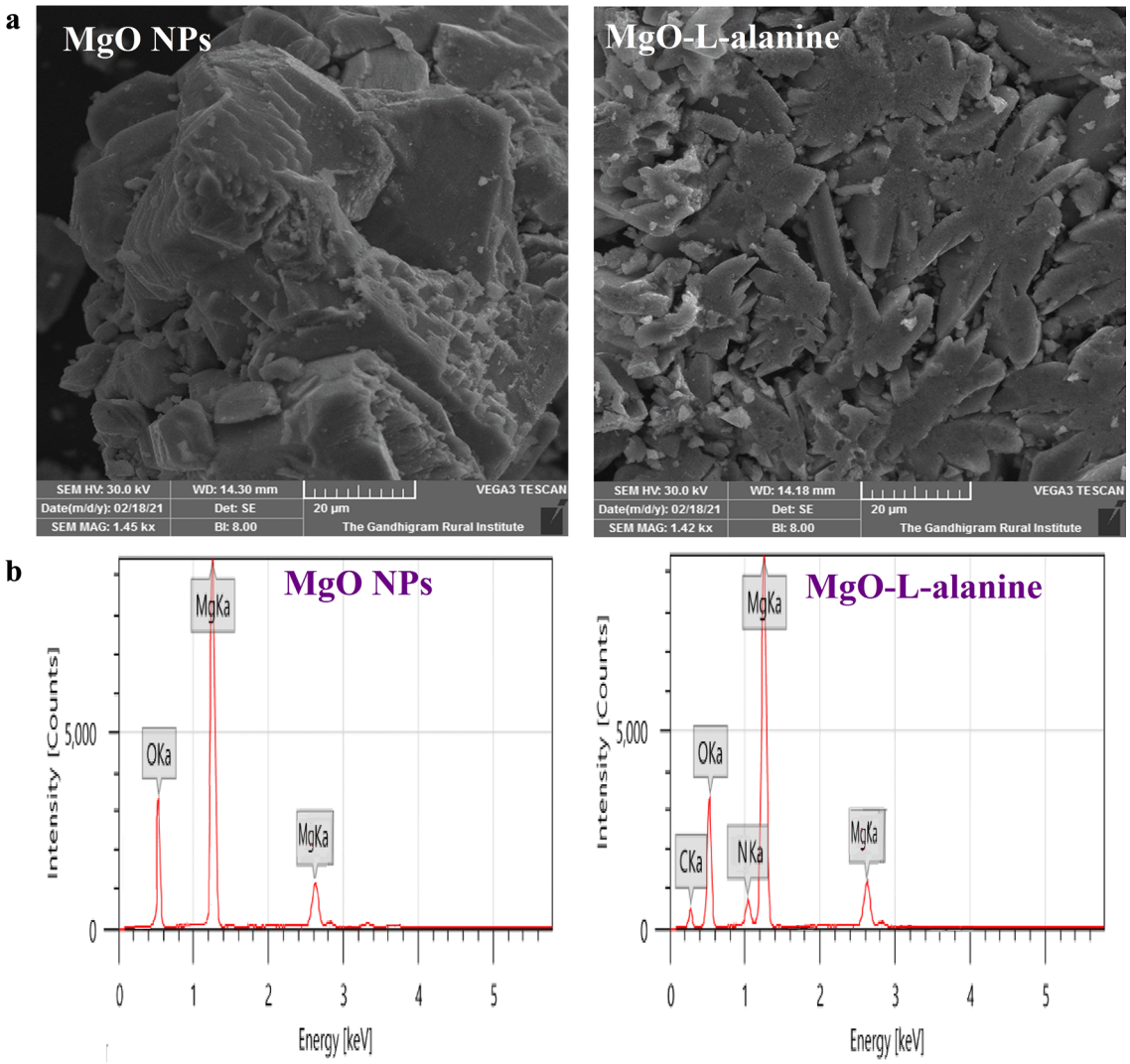

Fig. 5 **a** SEM images and **b** EDAX profile of prepared MgO NPs and MgO-L-alanine NPs

higher values [58], and PVA/CMC/MgO-L-alanine NCs film showed semi-crystalline structure.

3.4 Scanning Electron Microscopy (SEM) and Energy Dispersive X-ray (EDX)

It illustrates MgO nanoparticles are predominantly in plate-like shape and aggregate into larger particles size with no well-defined morphology (Fig. 5a) [22], and loosely arranged plate-like crystals are observed for the characteristic morphology of MgO nanoplates after surface modified with L-alanine (Fig. 5a). EDX was also utilized to examine the elemental profiles of NCs films containing MgO nanoplates and MgO-L-alanine nanoplates, and elemental mappings showed elemental distribution of each component (C, O, N, and Mg) in Fig. 5b. The results shows that, Mg and O are present in plain MgO nanoplates, while C, N, O, and Mg elements are uniformly dispersed in modified MgO-L-alanine [22]. A very smooth surface can be observed in pure PVA film. Similarly, microstructure images of the PVA/CMC blend appeared smooth and homogenous without pores or cracks indicating good compatibility between PVA and CMC to form films (Fig. 6a, b). This can be explained by a strong intermolecular association between the PVA and CMC. The PVA/CMC/MgO-L-alanine NCs film showed a distribution pattern of MgO-L-alanine and exhibited morphology of MgO-L-alanine up to 5 wt% in PVA/CMC system (Fig. 6c–e) [25]. It can be observed that, MgO-L-alanine is uniformly dispersed and plate-like structures indicated the presence of MgO-L-alanine in the main polymeric film. The plate-like structures tend to increase with increasing MgO-L-alanine content on NCs film. It was noticed that, the surface of the NCs film was dense and no cracks or

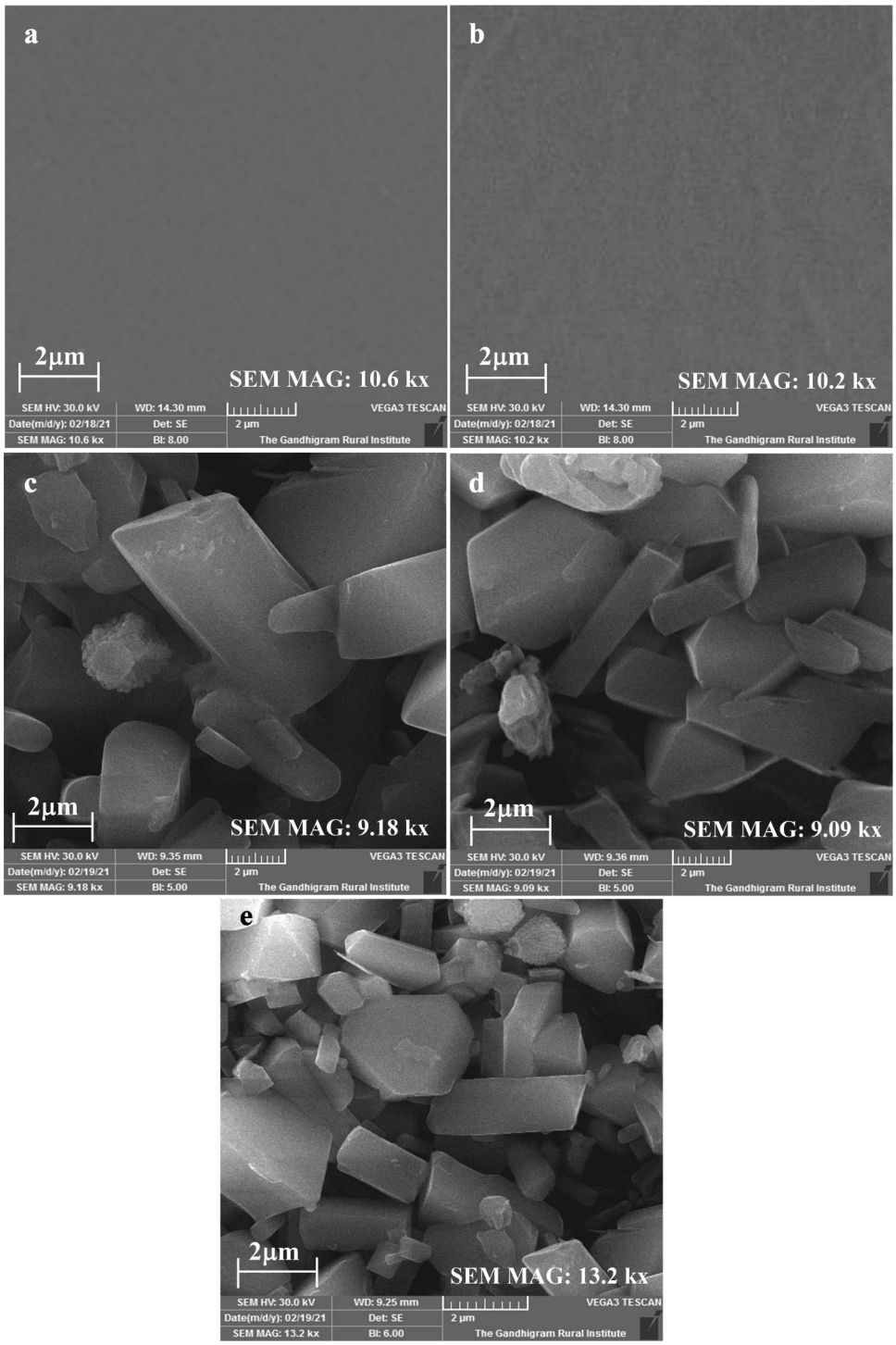

Fig. 6 SEM images of PVA (**a**), PVA/CMC (**b**), PCC-1 (**c**), PCC-2 (**d**), PCC-3 (**e**) and PCC-4 (**f**)

pores, were found up to 5% MgO-L-Ala, increased to 10% MgO-L-Ala resulted cracking of the film and broken film observed. The incorporation of MgO-L-alanine had a synergetic effect, resulting in a material with higher homogeneity. Hence, the SEM images of PVA/CMC/MgO-L-alanine showed smooth surfaces with consistently dispersed MgO-L-alanine in the main polymer PVA/CMC matrix.

3.5 Thermogravimetric Analysis (TGA)

Figure 7a shows the TGA curves of pure PVA, PVA/CMC, and PVA/CMC NCs films with different % of MgO-L-alanine contents. According to TGA thermograms, PVA, PVA/CMC, and PVA/CMC NCs films go through three distinct stages of thermal degradation [17]. The first stage

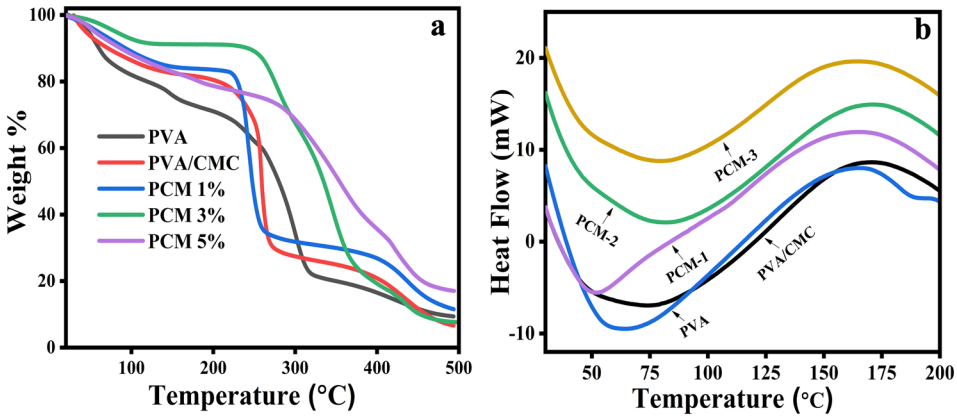

Fig. 7 TGA (**a**) and DSC (**b**) curves of prepared PVA, PVA/CMC and NCs films

Table 1 Thermal properties of pure PVA, PVA/CMC and PVA/CMC/MgO-L-alanine NCs

Sample code	TGA		DSC
	T_{10}^{a} (°C)	Char yield[b] [%]	Tg
PVA	130.11	5	53.31
PVA/CMC	133.23	12	51.25
PCM-1	93.75	17	54.75
PCM-2	92.12	20	87.64
PCM-3	90.84	25	95.51

[a]Temperature at which 10% weight loss was recorded by TGA at a heating rate of 10 °C/min^{-1} under nitrogen atmosphere

[b]Weight percentage of material left undecomposed after TGA at a temperature of 500 °C under nitrogen atmosphere

mass loss occurred between 50 and 230 °C, due to the evaporation of surface-adsorbed water responsible for the weight loss in 50–120 °C. At 120–230 °C, the weight loss is due to the volatilization of physical and chemically bonded water from the NCs films. The second stage of weight loss is induced by the degradation of the L-alanine amino acid, polymer dehydration, and the formation of a polyacetylene-like structure at temperatures between 230 and 340° C. From 340 to 500 °C, the third stage of weight loss is observed, which is caused by the thermal deterioration of PVA/CMC in the matrix. The pure PVA and PVA/CMC films showed 10% and 12% residue decompose at 500 °C respectively, while the weight percent remaining after major degradation at 470 °C for NCs (1, 3 and 5 wt%) is higher than the control PVA/CMC blend. PCM-1, PCM-2 and PCM-3 had 17%, 20% and 25% residue loss at 500 °C respectively. According to this result, PVA/CMC/MgO-L-alanine NCs films have higher thermal stability than the pure PVA/CMC and NCs 5 wt% could be optimized amount. Table 1 summarizes the TGA data for the NCs films prepared thermal degradation temperature.

3.6 Differential Scanning Calorimetry (DSC)

DSC is a characterization technique used to investigate polymer blends miscibility [46]. Figure 7b shows the DSC thermograms of PVA, PVA/CMC, and PVA/CMC/MgO-L-Ala NCs films, with the glass transition temperatures (Tg) values are mentioned in Table 1 [18]. The prepared neat PVA and PVA/CMC blend films were shown in a single Tg value, which suggests that the complete miscibility of the PVA and CMC. DSC thermograms were used to investigate the influence of MgO-L-alanine on the thermal characteristics of the PVA/CMC blend, and thermal parameters, such as glass transition temperature (Tg) was determined and listed in Table 1. As can be seen, increasing the MgO-L-alanine concentration in the PVA/CMC blend from 1 to 5 wt% enhanced the Tg value. The dispersion of MgO-L-alanine on the PVA/CMC blend, hydrogen bonding, and interaction of polymer chains with MgO-L-alanine all affect the Tg value of PVA/CMC NCs films [18]. The formation of strong hydrogen bonding between MgO-L-alanine and the PVA/CMC blend can inhibit polymer chain segmental mobility and hence boost Tg value.

3.7 Mechanical Property

During processing, transportation, distribution, retailing and storage, adequate mechanical strength and extensibility are necessary to protect the integrity and qualities of the foodstuff inside the package [31, 51]. The thickness and mechanical properties including tensile strength (TS), elongation at break percentage (E%), and elastic modulus (EM) of films based on a PVA/CMC blend as control and those reinforced with MgO-L-alanine (1, 3, and 5 wt%) are presented in Table 2. The thickness of the investigated films varied between 40 and 46 µm. The PVA/CMC blend showed the lowest thickness value while the incorporation of MgO-L-alanine significantly increased the thickness ($p < 0.05$) of the film due to the increase in the solid content. The

Table 2 Thickness (μm), Tensile strength (TS), elongation at break (EB), and tensile modulus (Y) of the prepared films

Sample code	Thickness (μm)	TS(MPa)	Y (GPa)	EB (%)
PVA	41.00 ± 1.0	16.12 ± 0.51	0.3911 ± 0.02	40.16 ± 0.9
PVA/CMC	41.32 ± 0.9	20.56 ± 0.74	0.3222 ± 0.02	35.45 ± 0.6
PCM-1	42.59 ± 1.6	21.89 ± 0.64	0.2973 ± 0.04	33.25 ± 0.7
PCM-2	45.74 ± 1.5	23.41 ± 0.85	0.2644 ± 0.03	32.50 ± 0.8
PCM-3	48.23 ± 1.1	23.79 ± 0.92	0.2516 ± 0.04	32.19 ± 0.4

mechanical properties of NCs films are affected by particle size and morphology, particle loading and distribution, the polymer matrix, and interfacial adhesion between MgO-L-alanine and polymers. The PVA/CMC/MgO-L-Ala NCs films had a higher tensile strength and E-modulus (Fig. 8a, b) than PVA/CMC, which may be due to the strong interfacial adhesion between MgO-L-alanine and PVA/CMC, as well as homogeneous dispersion of the modified MgO within the PVA/CMC matrix. Modified MgO nanoplates resulted in a significant decrease in EB values in the PVA/CMC film (Fig. 8a). The reduced EB values imply that PVA/CMC films became brittle after being compounded with MgO-L-alanine nanoplates, which played a role as bridge intercalating PVA/CMC chains. Furthermore, the mechanical strength of the NCs films may change depending on the degree of chain elongation and the nature of the L-alanine amino acid.

3.8 Soil Burial Degradation (SBD) of NCs

A Biodegradation investigation study is essential because of the environmental implications. To assess the biodegradability of the prepared bio-nanocomposite films under natural environmental circumstances, soil burial degradation tests were carried out [60]. The soil degradation of the prepared films in 10 days was shown in Fig. 9a. Neat PVA and PVA/CMC blend films possessed relatively good biodegradation tests. The soil degradability of neat PVA and PVA/CMC blend films was found to be 36.56 ± 1.08% and 40.43 ± 1.12% respectively, which suggests that blending CMC with PVA enhances the degradability. The presence of carbohydrate content (CMC) increases the soil degradability by providing a larger carbon source for bacteria that were activated by the addition of water and disrupted polymer interactions. Moreover, incorporation of MgO-L-alanine into the PVA/CMC matrix does negatively influence the soil degradability. The degradation percentage was found to be 38.93, 38.49, and 37.62% for PCM-1, PCM-2, and PCM-3, respectively. The NCs film containing higher MgO-L-alanine concentration showed lower soil degradation is mainly due to the microbial resistant capacity of MgO-L-alanine could resist the microbe activation and delayed the polymer chain disruption.

3.9 Moisture Retention Capacity (MRC)

Moisture retention capacity packaging systems, particularly in the form of food preservation films have a bright future ahead of them, since they are compatible with the food safety approach [55]. The moisture retention capacity of neat PVA, PVA/CMC, and PVA/CMC/MgO-L-alanine NCs films is shown in Fig. 9a. The MRC values ranged from 87 to 90%. The control film has higher MRC values than films containing MgO-L-alanine ($p < 0.05$), and the MRC value in the film was reduced by increasing the MgO-L-alanine concentration ($p < 0.05$). MRC of the PCM-1, PCM-2 and PCM-3 were increased by 0.84, 1.85 and 2.82% respectively, this could be due to the significant interaction of MgO-L-alanine with PVA/CMC chains, which results in a decrease in free hydroxyl group availability and, as a result, a decrease in hydrophilicity and MRC value.

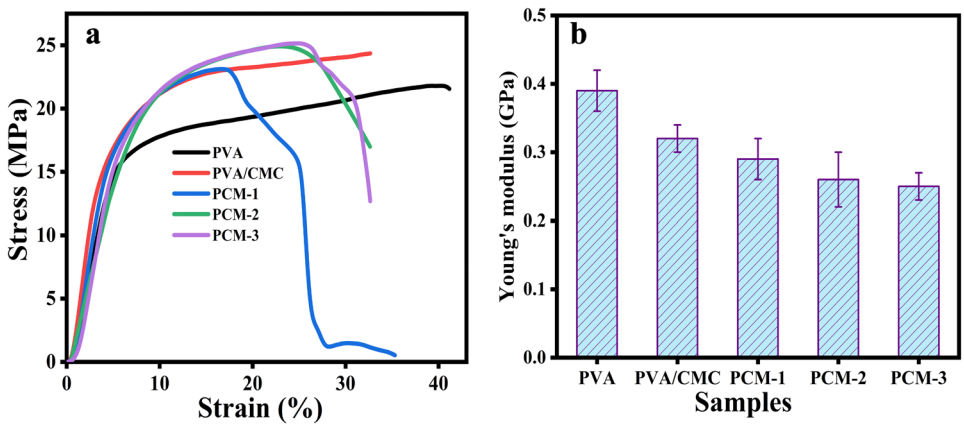

Fig. 8 Breaking stress and elongation at break (**a**) and Young's modulus (**b**) of PVA, PVA/CMC and NCs film (mean ± SD, n = 3)

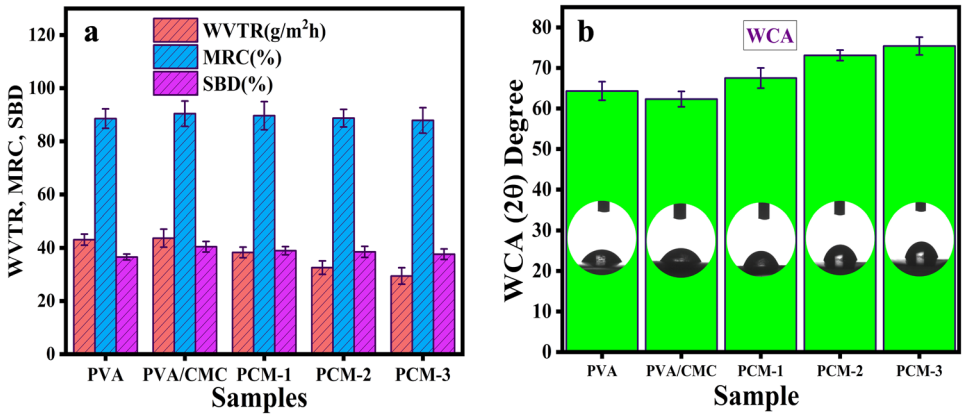

Fig. 9 WVTR, MRC and Soil burial degradation (**a**) and WCA (**b**) of PVA, PVA/CMC and NC films (mean ± SD, n = 3)

Table 3 Comparison of MRC, WVTR and TS testing of present work with others work

Samples	MRC (%)	WVTR (g/m^2 h)	TS (MPa)	References
PVA/St/Ag NPs Aq-100	97.6	50.2	25	[61]
PVA/St/GCN 0.18	96	90	24	[62]
Gelatin/PVA/Kaolin 0.25%	–	34	17.5	[63]
PVA/GA/GO	–	32.13	1.51	[53]
PVA/CMC/MgO-L-alanine 5%	87.85	29.43	23	Present work

MRC moisture retention capacity, *WVTR* water vapor transmission rate, *TS* tensile strength

3.10 Water Vapor Transmission Rate (WVTR) of NCs Films

The WVTR test is used to measure the water vapor diffusion rate from the surrounding environment to the matrix. WVTR evaluation is more important in packaging since it has a direct impact on the quality of the food contained within [56]. The WVTR values of neat PVA, PVA/CMC, and PVA/CMC/MgO-L-alanine NCs films were shown in Fig. 9a. The WVTR of the PVA and PVA/CMC was found to be 43.09 ± 2.06 and 43.65 ± 1.96 g m^{-1} h respectively. WVTR of the PCM-1, PCM-2 and PCM-3 were decreased by 12.27, 25.36 and 32.57% respectively, compared to PVA/CMC film. As it can be seen, WVTR of PVA/CMC NCs film reduced by MgO-L-alanine concentrations. The NCs film containing higher MgO-L-alanine concentration showed lower WVTR. The decreased in WVTR due to the addition of MgO-L-alanine can be attributed to the reduced hydrophilicity, which is caused by the decrease in the availability of free hydroxyl groups. In addition, the mobility of the polymer chains is reduced by the presence of MgO-L-alanine fillers in the PVA/CMC matrix, which reduces the diffusion speed of water vapor molecules. Table 3 represents some reports of PVA composite films that were compared with the present work [53, 61–63], which suggests that, the present prepared films showed very good WVTR properties compared to the others work reported, probably due to the effect of MgO-L-alnine.

3.11 Surface Wettability Test (SWT)

Low water contact angles of < 90◦ are associated with good material wettability, whereas high contact angles of > 90◦ are associated with low wettability. Similarly, lower water contact angles indicate the hydrophilic surface nature of the material, and higher water contact angles indicate the hydrophobic surface nature of the material [6]. The water contact angle of neat PVA, PVA/CMC blend, and PVA/CMC/MgO-L-alanine NCs films were shown in the Fig. 9b. The WCA of the neat PVA film was 65.59 ± 1.6°, which was decreased to 62.73 ± 2.0° by the addition of CMC, indicating an increased in hydrophilicity of the films. The decreased WCA was attributed to the hydrophilic nature of the CMC. WCA of PCM-1, PCM-2 and PCM-3 was increased by 8.34, 14.77 and 17.37%, compared to PVA/CMC film respectively. As it can be seen WCA of PVA/CMC was reduced with increasing MgO-L-alanine concentrations. The film containing a higher concentration of MgO-L-alanine (PCM-3) showed higher WCA. This is due to the comparatively high hydrophobic character of MgO-L-alanine with a low number of hydroxyl groups, which resulted in a decreased in water absorption capacity, resulting in less hydrophilic nature of the nanocomposite film surfaces.

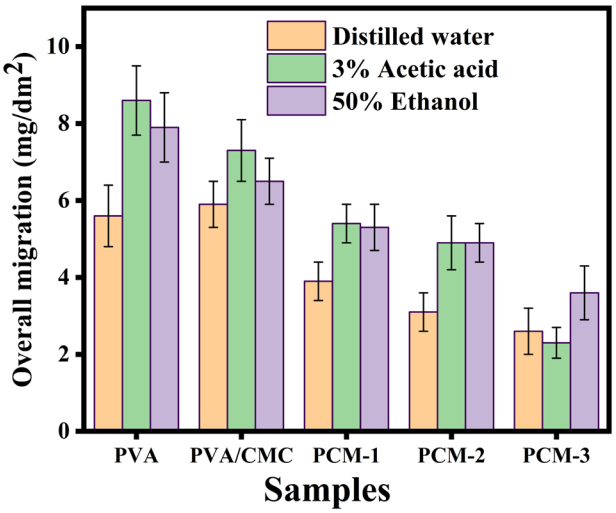

Fig. 10 Overall migration rate (food compatibility) of PVA, PVA/CMC and NC films (mean ± SD, n = 3)

3.12 Overall Migration Rate (OMR)

In food packaging, migration process is crucial since the non-intended transfer of unwanted packaging constituents may affect the food safety for the consumer. Further in NCs film food packaging, nanomaterials may migrate into the food and migrated nanomaterials could eventually induce quality changes of the foods and also contaminants. Therefore, it is necessary to carry out migration analysis for food packaging use [6]. The overall migration rates of PVA/CMC blend and its corresponding NCs films at different MgO-L-alanine contents were evaluated in three food simulants such as distilled water, acetic acid, and ethanol which imitate the aqueous foods, acidic foods, and alcoholic beverages, respectively. The MgO-L-alanine content migration from the PVA/CMC matrix profile was shown in Fig. 10. The migration rate of the MgO-L-alanine into the 3% acetic acid was found to be the highest followed by 50% ethanol and distilled water. The increase in the migration rate in the 3% acetic acid simulant is attributed to the increased interaction of PVA/CMC chains with water molecules in the presence of acidic media, hence increased MgO-L-alanine. Among other simulants, the higher release in 50% ethanol simulant is attributed to the more hydrophobic character of the NCs. The MgO-L-alanine incorporated PVA/CMC NCs film showed overall migration rates within the acceptable limit of 10 mg/dm^2. The migration rate of all films (PVA/CMC and NCs) was significantly ($p < 0.05$) reduced by the influence of MgO-L-alanine. The closed dense polymeric network formed by the addition of MgO-L-alanine may lead to a reduction in the migration rate. The results demonstrated that, NCs and PVA/CMC matrices had strong interfacial bonding between them caused reduction in the migration while exposed to stimulants [6].

3.13 Antioxidant Property

Antioxidant active packaging is a novel method of enhancing the stability of the oxidation-sensitive foods. Their functions include the release of the antioxidant agents, and the reduction of reactive oxygen species (ROS) [5]. Figure 11a. shows the antioxidant activity percentage (%) and half-maximal inhibitory concentration (IC_{50}) of the developed composite film samples. L-Alanine content present in the PVA/CMC NCs film was responsible for the free radical scavenging activity. The % DPPH scavenging activity of MgO-L-alanine incorporated PVA/CMC NCs film considerably increased with the increase in the concentrations of the sample, where the neat PVA and PVA/CMC blend film shows negligible antioxidant activity. PVA/CMC NCs film showed significantly ($p < 0.05$) improved % DPPH scavenging activity which is due to the presence of L-alanine content for the free radical scavenging of DPPH, Grosser et al. investigated the antioxidant activity of the L-alanine amino acid. The PCM-3 film exhibited higher (58.12%) radical scavenging activity in contrast with other films. The IC_{50} values of 10–50, 50–100,

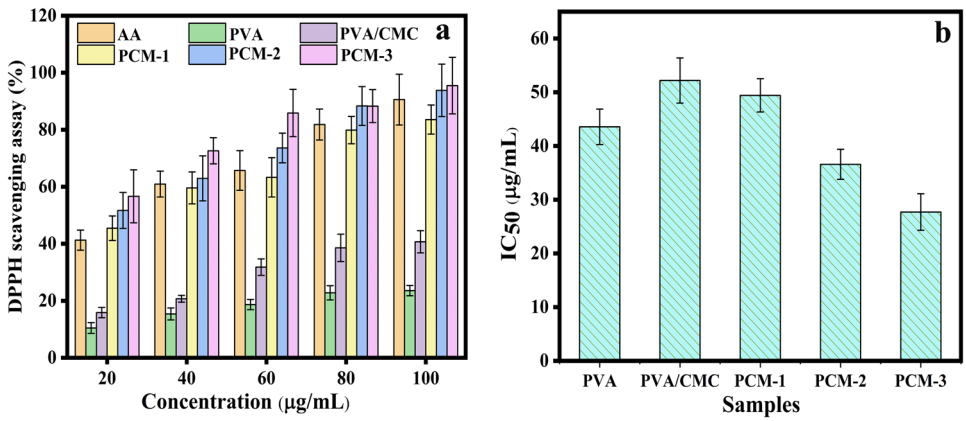

Fig. 11 Antioxidant profile (**a**) and IC_{50} value of prepared PVA, PVA/CMC and NCs films (**b**) (mean ± SD, n = 3) *AA Ascorbic acid

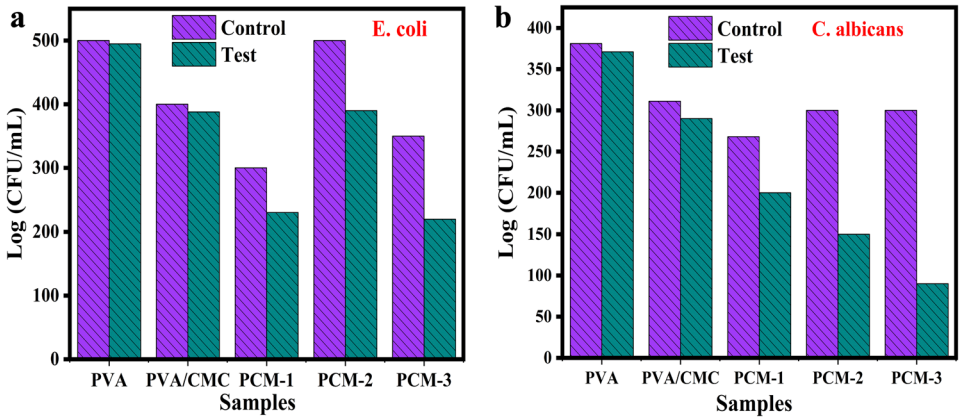

Fig. 12 Log CFU/ mL of PVA, PVA/CMC and NCs films against *E. coli* (**a**), *S. aureus* (**b**), *C. albicans* (**c**) and *C. tropicalis* (**d**)

and > 100 g/mL respectively indicated strong, moderate, and weak antioxidant activity. The IC_{50} values of the PVA/CMC NCs films from non-blended to blended and NCs doped exhibited gradual increased antioxidant activity (Fig. 11b) [5].

3.14 Antibacterial and Antifungal Activity

Antimicrobial characteristics are desirable in a food packaging material to reduce bacteria development in food [57]. The total colony count method was used to examine the antibacterial properties of neat PVA, PVA/CMC, and PVA/CMC/MgO-L-alanine films against Gram-negative *E. coli*, and the log CFU/mL of each film was plotted (Fig. 12a). The antibacterial activity of the neat PVA film as well as the PVA/CMC films showed poor inhibition against the test organisms. Meanwhile, the films containing MgO-L-alanine have shown very good antibacterial activity against *E. coli* bacteria, and as the concentration of MgO-L-alanine in the NCs increased. It revealed, the antibacterial activity was directly dependent on the concentration of MgO-L-alanine in the nanocomposite films. This is owing to the presence of nanosized magnesium oxide in the polymer blend inhibit the reactive oxygen species (ROS). The NCs material present in the film interact with the cell membrane of the bacteria and penetrate the cell, causing bacterial cell growth to be inhibited and perhaps leading to death. Magnesium oxide nanoparticles also destroy DNA and proteins of the bacteria, hinder biofilm formation, harm proton efflux pumps, and oxidize the cellular components of the bacteria studies are reported.

The colony count method was used to assess the antifungal activity of the films, and the log CFU/mL of each film was plotted (Fig. 12b) [57]. The PVA and PVA/CMC films had very low growth inhibition against *Candida albicans*, according to the findings. Films containing MgO-L-alanine showed very good growth inhibition against *C. albicans* fungus, as the concentration of MgO-L-alanine in the NCs increases. It suggests that, the activity was dependent on the concentration of the MgO-L-alanine present in the NCs film. These studies revealed, the content of nanosized magnesium oxide present in the polymer blend is responsible for the antifungal activity. The mechanism of action mainly involves cell membrane damage, disruption of energy metabolism, generation of oxidative stress due to reactive oxygen species formation, and inhibition of the transcription by NCs.

4 Conclusion

In the present work, for the first time, we are synthesized MgO NPs from agro-waste WELFSA, and prepared MgO have been functionalized by the amino acid L-alanine using microwave irradiation, and finally incorporated into PVA/CMC blend to form nanocomposite films. ATR/FT-IR spectroscopy indicated strong interactions via H-bonds between the PVA and CMC chains and MgO-L-alanine involved. In addition, FT-IR-ATR analysis confirms that, the incorporation of different contents of the MgO-L-alanine enhances the stretching of the polymeric backbone chains. The XRD and SEM analysis suggested crystallinity and homogeneous dispersion of MgO-L-alanine in the PVA/CMC matrix present in the film. The thermogravimetric analysis showed, three stages of thermal decomposition of the films pure PVA, PVA/CMC, and PV/CMC/MgO-L-alanine NCs. PCM-3 film showed higher thermal stability than any other films studied in this work. Through DSC analysis, it was observed that, the incorporation of different content of MgO-L-alanine in the PVA/CMC matrix increases the degree of crystallinity, obtained results are well-matched with XRD analyses. The incorporation of MgO-L-alanine significantly enhanced mechanical properties such as tensile strength and Young's modulus of PVA/CMC NCs film. Also, MgO-L-alanine incorporated films exhibited excellent UV light screening properties with remarkable antimicrobial activity against food-borne pathogens *E. coli* and *C. tropical*.

Moreover, within 10 days, the prepared films exhibited a soil degradation rate more than 30%. The prepared NCs films were discovered to have a good moisture retention capability, making them promising for fresh fruits and vegetables packaging with a high rate of respiration. Together with the formation of hydrogen bonds between polymeric matrices and nanofillers (increase of MgO-L-Ala content increased hydrophobic nature of the film), may prevent water molecule migration across polymer matrices. The incorporation of MgO-L-alanine decreased the hydrophilic nature of the prepared nanocomposite films, which was indicated by increasing the water contact angle of nanocomposite films by 17.37% to PVA/CMC blend films. The antioxidant activities of the PVA/CMC/MgO-L-alanine NCs films *in-vitro* studies clearly revealed the NCs films showed stronger scavenging effect than control PVA/CMC film. These results suggested that, these nanocomposite films could be employed to reduce oxidative stress as a component in health or functional foods. Furthermore, the acceptable food packaging properties such as good transparency and overall water migration characteristics can be observed in the PVA/CMC/MgO-L-alanine NCs film. Hence, all in all, it can be concluded that, our current research work outputs and deliverables are expected to serve as a very good platform in food packaging applications.

Supplementary Information The online version contains supplementary material available at https://doi.org/10.1007/s10904-022-02261-9.

Acknowledgements Authors are thankful to UGC for the award of Major Research Project and VGST, Govt. of Karnataka for SMYSR award and K-FIST-Level-II for financial support to KK.

Author Contributions YA: Conceptualization; Data curation; Formal analysis; Methodology; Resources; Software; Roles: Writing—original draft. TG: Data curation, formal analysis; Role: Writing original draft. KK: The corresponding author; Investigation; Supervision; Validation; Visualization; Role: Review & editing.

Declarations

Competing interest All authors declare that they have no conflict of interest.

References

1. Y. Chen, A.K. Awasthi, F. Wei, Q. Tan, J. Li, Sci. Total Environ. **752**, 141772 (2021)
2. R. Katakojwala, S.V. Mohan, Curr. Opin. Green Sustain. Chem. **27**, 100392 (2021)
3. P. Chaudhary, F. Fatima, A. Kumar, J. Inorg. Organomet. Polym. Mater. **30**, 5180 (2020)
4. J. Jacob, S. Gopi, *Isolation and Physicochemical Characterization of Biopolymers* (Elsevier, Amsterdam, 2021)
5. T. Gasti, S. Dixit, O.J. D'souza, V.D. Hiremani, S.K. Vootla, S.P. Masti, R.B. Chougale, R.B. Malabadi, Int. J. Biol. Macromol. **187**, 451 (2021)
6. T. Gasti, S. Dixit, V.D. Hiremani, R.B. Chougale, S.P. Masti, S.K. Vootla, B.S. Mudigoudra, Carbohydr. Polym. **277**, 118866 (2022)
7. O.F. Nwabor, S. Singh, S. Paosen, K. Vongkamjan, S.P. Voravuthikunchai, Food Biosci. **36**, 100609 (2020)
8. N. Jain, V.K. Singh, S. Chauhan, J. Mech. Behav. Mater. **26**, 213 (2017)
9. A. Barman, A. De, M. Das, J. Inorg. Organomet. Polym. Mater. **30**, 2248 (2020)
10. K.M. Amin, A.M. Partila, H.A. Abd El-Rehim, N.M. Deghiedy, Part. Part. Syst. Charact. **37**, 2000006 (2020)
11. C.C. Demerlis, D.R. Schoneker, Food Chem. Toxicol. **41**, 319 (2003)
12. X. Tang, S. Alavi, Carbohydr. Polym. **85**, 7 (2011)
13. T. Gasti, S. Dixit, S.P. Sataraddi, V.D. Hiremani, S.P. Masti, R.B. Chougale, R.B. Malabadi, J. Polym. Environ. **28**, 2918 (2020)
14. S. Hajji, R.B.S. Ben Salem, M. Hamdi, K. Jellouli, W. Ayadi, M. Nasri, S. Boufi, Process Saf. Environ. Prot. **111**, 112 (2017)
15. J. Kowalonek, H. Kaczmarek, A. Dbrowska, Appl. Surf. Sci. **257**, 325 (2010)
16. H. Haghighi, M. Gullo, S. LaChina, F. Pfeifer, H.W. Siesler, F. Licciardello, A. Pulvirenti, Food Hydrocolloids **113**, 106454 (2021)
17. E. Dhandapani, S. Suganthi, S. Vignesh, M. Dhanalakshmi, J. Kalyana Sundar, V. Raj, Mater. Technol. **00**, 1 (2020)
18. P. V. A. Cmc, C. Film, and C. Wang, 1 (2020).
19. S. El-Gamal, A.M. El Sayed, E.E. Abdel-Hady, J. Polym. Environ. **26**, 2536 (2018)
20. J.S. Behra, J. Mattsson, O.J. Cayre, E.S.J. Robles, H. Tang, T.N. Hunter, ACS Appl. Polym. Mater. **1**, 344 (2019)
21. A.M. El Sayed, S. El-Gamal, W.M. Morsi, G. Mohammed, J. Mater. Sci. **50**, 4717 (2015)
22. A.M. Youssef, F.M. Assem, H.S. El-Sayed, S.M. El-Sayed, M. Elaaser, M.H. Abd El-Salam, RSC Adv. **10**, 37857 (2020)
23. H.S. Roy, M.Y.A. Mollah, M.M. Islam, M.A.B.H. Susan, Polym. Bull. **75**, 5629 (2018)
24. M. Li, F. Chen, C. Liu, J. Qian, Z. Wu, Z. Chen, J. Inorg. Organomet. Polym Mater. **29**, 1738 (2019)
25. H. Helmiyati, Z.S.Z. Hidayat, I.F.R. Sitanggang, D. Liftyawati, Polym. Test. **104**, 107412 (2021)
26. B. Darbasizadeh, Y. Fatahi, B. Feyzi-barnaji, M. Arabi, H. Motasadizadeh, H. Farhadnejad, F. Moraffah, N. Rabiee, Int. J. Biol. Macromol. **141**, 1137 (2019)
27. Z. Guo, D. Zhang, S. Wei, Z. Wang, A.B. Karki, Y. Li, P. Bernazzani, D.P. Young, J.A. Gomes, D.L. Cocke, T.C. Ho, J. Nanopart. Res. **12**, 2415 (2010)
28. S.F. Bdewi, O.G. Abdullah, B.K. Aziz, A.A.R. Mutar, J. Inorg. Organomet. Polym. Mater. **26**, 326 (2016)
29. G. Magesh, G. Bhoopathi, N. Nithya, A.P. Arun, E. Ranjith Kumar, J. Inorg. Organomet. Polym Mater. **28**, 1528 (2018)
30. F. Mustafa, S. Andreescu, RSC Adv. **10**, 19309 (2020)
31. T. Gasti, V.D. Hiremani, S.S. Kesti, V.N. Vanjeri, N. Goudar, S.P. Masti, S.C. Thimmappa, R.B. Chougale, J. Polym. Environ. **29**, 3347–3363 (2021)
32. S. Zinatloo-Ajabshir, M.S. Morassaei, M. Salavati-Niasari, Compos. B Eng. **167**, 643 (2019)
33. S. Zinatloo-Ajabshir, N. Ghasemian, M. Mousavi-Kamazani, M. Salavati-Niasari, Ultrason. Sonochem. **71**, 105376 (2021)
34. S.M. Tabatabaeinejad, S. Zinatloo-Ajabshir, O. Amiri, M. Salavati-Niasari, RSC Adv. **11**, 40100 (2021)
35. S. Zinatloo-Ajabshir, M.S. Morassaei, O. Amiri, M. Salavati-Niasari, Ceram. Int. **46**, 6095 (2020)

36. H. Safajou, M. Ghanbari, O. Amiri, H. Khojasteh, F. Namvar, S. Zinatloo-Ajabshir, M. Salavati-Niasari, Int. J. Hydrog. Energy **46**, 20534 (2021)
37. S. Zinatloo-Ajabshir, M.S. Morassaei, O. Amiri, M. Salavati-Niasari, L.K. Foong, Ceram. Int. **46**, 17186 (2020)
38. F. Razi, S. Zinatloo-Ajabshir, M. Salavati-Niasari, Mater. Lett. **193**, 9 (2017)
39. S. Zinatloo-Ajabshir, M.S. Morassaei, M. Salavati-Niasari, J. Colloid Interface Sci. **497**, 298 (2017)
40. S. Zinatloo-Ajabshir, M. Salavati-Niasari, Compos. Part B: Eng. **174**, 106930 (2019)
41. S. Zinatloo-Ajabshir, Z. Salehi, O. Amiri, M. Salavati-Niasari, J. Alloy. Compd. **791**, 792 (2019)
42. T. Baysal, N. Noor, A. Demir, Polym.-Plast. Technol. Mater. **59**, 1522 (2020)
43. S. Abinaya, H.P. Kavitha, M. Prakash, A. Muthukrishnaraj, Sustain. Chem. Pharm. **19**, 100368 (2021)
44. S.K. Das, T. Parandhaman, M.D. Dey, Green Chem. **23**, 629 (2021)
45. L.H. Tagle, C.A. Terraza, H. Villagra, A. Tundidor-Camba, Polym. Bull. **67**, 1799 (2011)
46. N. Grosser, S. Oberle, G. Berndt, K. Erdmann, A. Hemmerle, H. Schröder, Biochem. Biophys. Res. Commun. **314**, 351 (2004)
47. A. Lopez-Arvizu, D. Rocha-Mendoza, E. Ponce-Alquicira, I. García-Cano, World J. Microbiol. Biotechnol. **37**, 1–13 (2021)
48. G.H. Park, M.S. Kang, J.C. Knowles, M.S. Gong, J. Biomater. Appl. **30**, 1350 (2016)
49. S.U. Dandare, I.J. Ezeonwumelu, T.S. Shinkafi, U.F. Magaji, A.A.I. Adio, K. Ahmad, J. Food Biochem. **45**, 1 (2021)
50. K. Kantharaju, S.Y. Khatavi, ChemistrySelect **3**, 5016 (2018)
51. S. Mallakpour, A. Nezamzadeh Ezhieh, Carbohydr. Polym. **166**, 377 (2017)
52. T. Gasti, V.D. Hiremani, S.P. Sataraddi, V.N. Vanjeri, N. Goudar, S.P. Masti, R.B. Chougale, R.B. Malabadi, Chem. Data Collect. **33**, 100684 (2021)
53. S. Chowdhury, Y.L. Teoh, K.M. Ong, N.S. Rafflisman Zaidi, S.K. Mah, Food Packag. Shelf Life **24**, 100463 (2020)
54. F. Luzi, E. Fortunati, A. Di Michele, E. Pannucci, E. Botticella, L. Santi, J.M. Kenny, L. Torre, R. Bernini, Carbohydr. Polym. **193**, 239 (2018)
55. K.K. Gaikwad, S. Singh, A. Ajji, Environ. Chem. Lett. **17**, 609 (2019)
56. M.S. Sarwar, M.B.K. Niazi, Z. Jahan, T. Ahmad, A. Hussain, Carbohyd. Polym. **184**, 453 (2018)
57. S. Mathew, J. Mathew, E.K. Radhakrishnan, J. Polym. Res. **26**, 1 (2019)
58. A. Ansari, A.A. Ali, M. Asif, Shamsuzzaman, I. Capek **9**, 1 (2019)
59. R. Bhuvaneshwari, S. Karthikeyan, N. Rajeswari, S. Selvasekarapandian, C. Sanjeeviraja, Solid State Ion. 543 (2012)
60. R. Anugrahwidya, B. Armynah, D. Tahir, J. Polym. Environ. **29**, 3459 (2021)
61. S. Batool, Z. Hussain, M.B.K. Niazi, U. Liaqat, M. Afzal, J. Drug Deliv. Sci. Technol. **52**, 403 (2019)
62. A. Ahmed, M.B.K. Niazi, Z. Jahan, G. Samin, E. Pervaiz, A. Hussain, M.T. Mehran, J. Polym. Environ. **28**, 100 (2020)
63. M. Shrungi, A. Goswami, J. Bajpai, A.K. Bajpai, Polym. Bull. **76**, 5791 (2019)